Research Article

Shuying Chen*, Qingchun Li, Ming Sun, Jiajian Song, Haiqing Sun, and Guowei Chang

Study on the effect of micro-shrinkage porosity on the ultra-low temperature toughness of ferritic ductile iron

https://doi.org/10.1515/htmp-2022-0238 received February 26, 2022; accepted August 23, 2022

Abstract: In this study, the ductile iron ingots are cast using a metal mold, and the riser neck diameter is changed to control the micro-shrinkage porosity, which can affect the ultra-low temperature toughness of ferritic ductile iron. The metallographic structure and microshrinkage porosity were observed by an Axiovert200 MAT measurer metallographic microscope and an MLA 250 (FEI quanta) scanning electron microscope, and the number and diameter of graphite nodules and microshrinkage porosity size were measured by Nano Measurer 1.2 software. The effect of micro-shrinkage porosity on the ultra-low temperature toughness of ferritic ductile iron was studied. It is found that the impact energy of ductile iron decreases with the increase of micro-shrinkage porosity size, and the influence of micro-shrinkage porosity is more obvious with the decrease of temperature. The results point out that the micro-shrinkage porosity becomes the key factor affecting the ultra-low temperature impact toughness of ductile iron when the spheroidization rate of ferritic ductile iron is greater than 98% and the number of graphite nodules is more than 810 mm⁻². The impact energy of ferritic ductile iron can still reach more than 12 J at -70°C when the length of micro-shrinkage porosity is less than 3.7 µm.

Keywords: ferritic ductile iron, micro-shrinkage porosity, ultra-low temperature, impact toughness

With the increasing usage of ductile iron in wind power generation, rail transit, nuclear power, large ships and other fields, the requirements for the mechanical properties of ductile iron, especially low-temperature impact toughness, are becoming increasingly stringent [1,2]. Therefore, people have carried out in-depth research on low-temperature and high-toughness ductile iron. Their primary research focuses on strengthening the morphology of graphite nodules [3-9] and alloying them [10-14]. Mechanical properties, casting defects, and heat treatment of nodular cast iron are also studied [15-21]. The research has made remarkable progress, and the production technology of low-temperature and high-toughness ductile iron has been successfully developed. Ductile iron has a strength larger than 400 MPa, an elongation greater than 18%, and an impact energy greater than 12 J at -40°C. However, when the temperature is lower than −60°C, it is difficult for the impact energy to exceed 10 J.

During the solidification process of ductile iron, it is easy for micro-shrinkage porosity to form between the austenite rings surrounding the graphite nodule. The micro-shrinkage porosity often has sharp corners, which will promote the crack initiation of ductile material, during low-temperature fracture. However, no one has yet noticed the effect of micro-shrinkage porosity on ductile iron's low-temperature toughness.

Therefore, the effect of micro-shrinkage porosity on the impact energy of ductile iron below –40°C is studied in this article, which can provide a theoretical basis for the production of ultra-low temperature ductile iron.

Qingchun Li, Guowei Chang: School of Materials Science and Engineering, Liaoning University of Technology, Jinzhou 121001, China

Ming Sun, Jiajian Song, Haiqing Sun: Department of Technology, Jinzhou Jietong Railway Machinery Manufacturing Co. Ltd, Jinzhou 121001, China

1 Experiment

The furnace burden of cast iron and scrap steel is melted using a 500 kg medium frequency induction furnace, and the tapping temperature of molten iron is 1,510–1,530°C. The pour-over spheroidizing treatment was carried out by using Fe-46Si-6Mg-1RE alloy as the spheroidizing agent. The secondary inoculation treatment was carried out by

^{*} Corresponding author: Shuying Chen, School of Materials Science and Engineering, Liaoning University of Technology, Jinzhou 121001, China, e-mail: jinzhouchenshuying@126.com

| Table 1: Chemical con | npositions of raw | materials and | ductile iron f | or the ex | periment (| wt%) |
|-----------------------|-------------------|---------------|----------------|-----------|------------|------|
| | | | | | | |

| | С | Si | Mn | Р | S | RE | Mg | Ва | Ti | Ca | Al | 0 |
|---------------------|-----|-------|-------|-------|------|-----------|-----------|---------|-------|-----------|-----------|------|
| Cast iron | 4.6 | 0.44 | 0.026 | 0.025 | 0.02 | | | | 0.03 | | | |
| Scrap steel | 0.2 | 0.26 | 0.54 | 0.04 | 0.05 | | | | | | | |
| Spheroidizing agent | | 44-48 | | | | 0.85-1.15 | 5.55-6.15 | | | 0.8-1.2 | ≤1.0 | |
| Si-Ba inoculant | | 72-78 | | | | | | 2.0-3.0 | | 1.0-2.0 | ≤1.5 | |
| S-O inoculant | | 70-76 | | | ≤1.0 | 1.5-2.0 | | | | 0.75-1.25 | 0.75-1.25 | ≤1.0 |
| Ductile iron | 3.8 | 2.2 | 0.15 | 0.025 | 0.01 | 0.02 | 0.04 | | 0.023 | | | |

using Silicon-Barium pregnant agent, and the flow inoculation treatment was carried out by using sulfur–oxygen pregnant agent. The pouring temperature ranges between 1,380 and 1,440°C. The chemical compositions of the experimental raw materials and ductile iron are shown in Table 1.

524

The ingots are poured using the method illustrated in Figure 1, with two ingots poured into each furnace. The pressure due to graphite expansion is controlled by graphitization in the ingot by altering the riser neck diameter $\phi\,A$ shown in Figure 1 to adjust the micro-shrinkage porosity in the ingot.

The ingot was kept at 740°C for 4 h to obtain ductile iron with a 100% ferrite matrix. The size of the impact specimen with a V-notch specimen is $10 \text{ mm}^3 \times 10 \text{ mm}^3 \times 55 \text{ mm}^3$. The sampling method is shown in Figure 1. Using the JB-50 impact testing machine, the impact energy of the impact specimen was tested at -40, -50, -60 and -70°C. Taking the metallographic sample from the punched sample, the

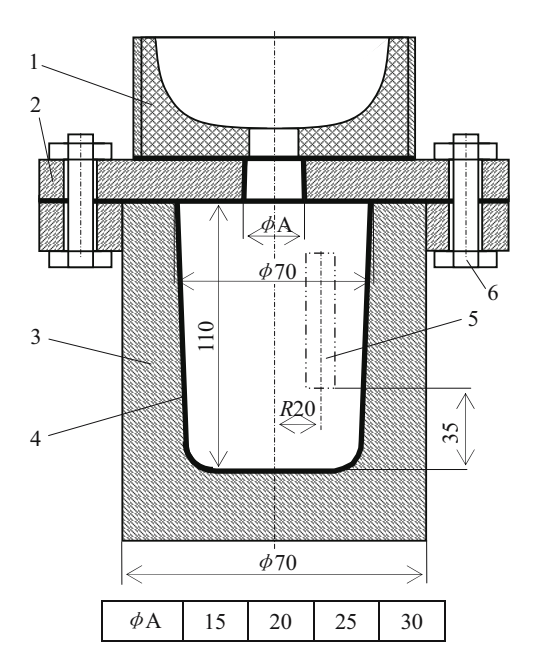


Figure 1: Pouring method of ingot. 1 – pouring cup; 2 – upper cover of ingot mold; 3 – ingot mold; 4 – coating; 5 – impact specimen; 6 – clamp bolt.

metallographic structure and micro-shrinkage porosity were observed with the Axiovert 200 MAT metallographic microscope and the MLA 250 (Fei quanta) scanning electron microscope, and the number and diameter of graphite nodules and the size of micro-shrinkage porosity were measured with Nano Measurer 1.2 software.

2 Experimental results and analysis

2.1 Metallographic structure

The metallographic structure after heat treatment is shown in Figure 2. The graphite nodules in the microstructure are fine, round, and evenly distributed, and the spheroidization rate can reach more than 98%.

The test results for the number and diameter of graphite nodules are shown in Figure 3. The number of graphite spheres per square millimeter ranges from 835 to 1,089, which ranges from 835 to 884 square millimeters mostly, as shown in Figure 3(a). The average diameter of a graphite ball is $13.2–14.8\,\mu\text{m}$, as shown in Figure 3(a); the number of graphite with $10–14\,\mu\text{m}$ is larger and the number of graphite nodule with 2–6 and $22–30\,\mu\text{m}$ is smaller, as shown in Figure 3(b); and the size of graphite nodule is relatively uniform.

The metal substrate consists of 100% ferrite after heat treatment. The average grain size of ferrite is about 37.9 μ m, and the size is relatively uniform, as shown in Figure 2.

2.2 Micro-shrinkage porosity

2.2.1 Effect of riser neck diameter on micro-shrinkage porosity

The SEM images of metallographic samples on the same radius of the ingot are shown in Figure 4, which reveal the micro-shrinkage porosity on the ferrite matrix. There

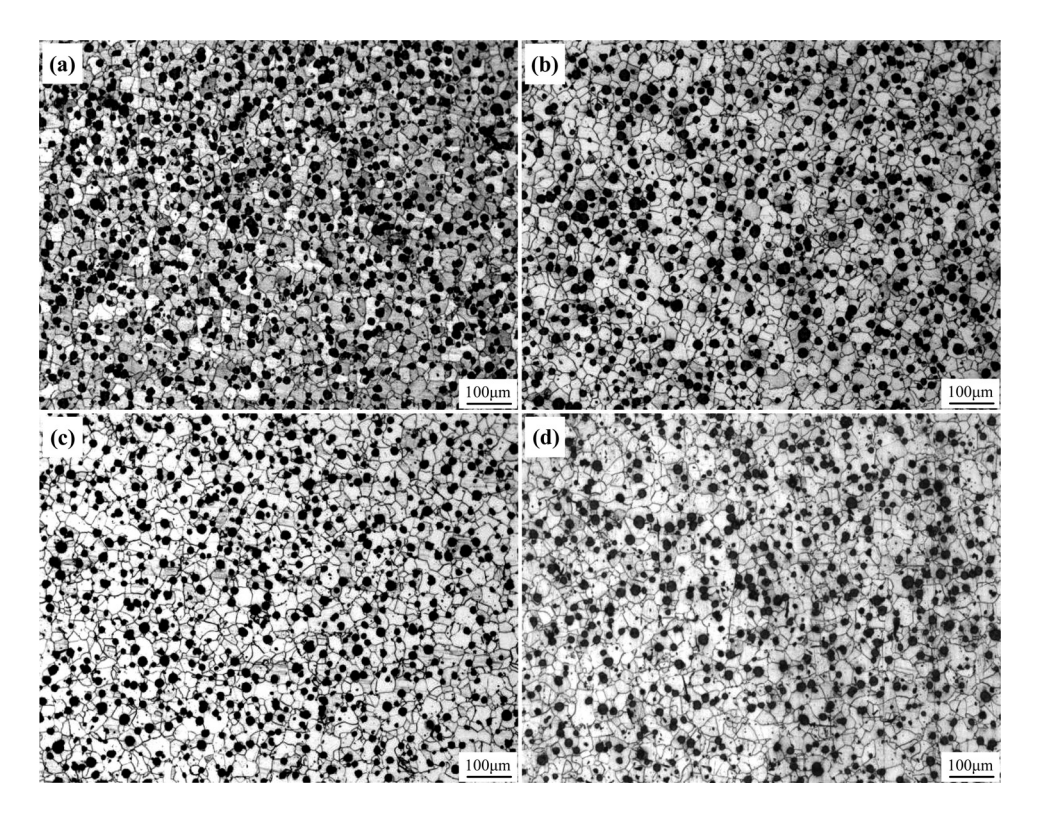


Figure 2: Metallographic structure (a) $\varphi A = 15$; (b) $\varphi A = 20$; (c) $\varphi A = 25$; and (d) $\varphi A = 30$.

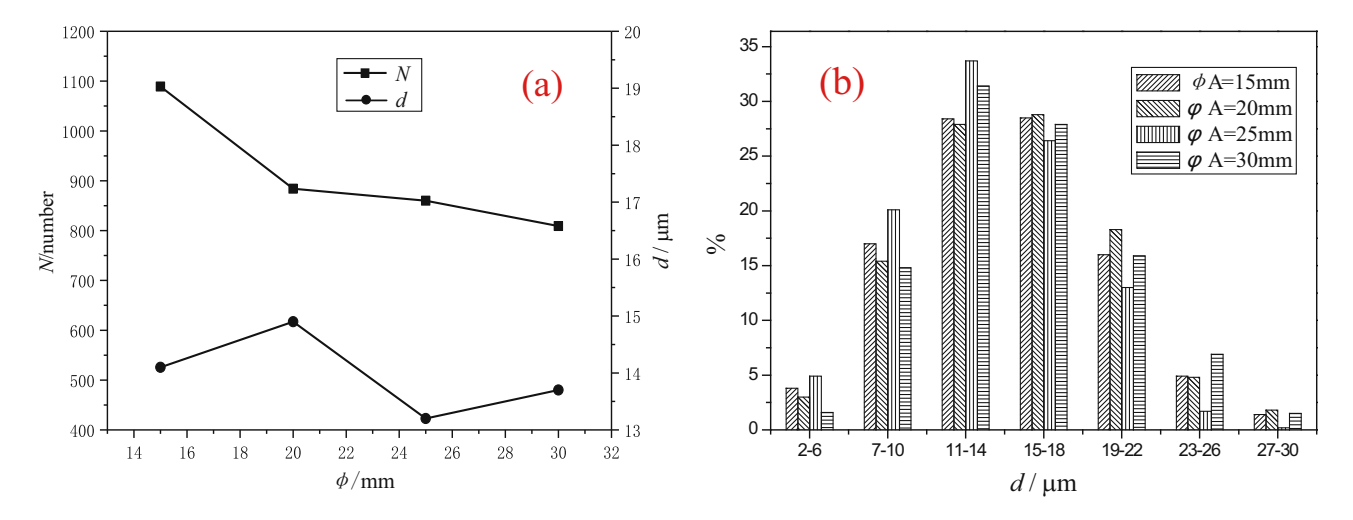


Figure 3: Graphite nodules: (a) number and diameter; (b) size distribution.

are mainly two kinds of micro-shrinkage porosity: triangular micro-shrinkage porosity (shown by the white arrow in Figure 4) and non-triangular micro-shrinkage porosity (shown by the black arrow in Figure 4). The sharp corner of triangular micro-shrinkage porosity is very sharp, and the radius of curvature of its tip is approximately zero. Other micro-shrinkage porosities have sharp corners as well, but it is not obvious. The radius of curvature of the tip of the non-triangular micro-shrinkage porosity is much larger

than that of the tip of the triangular micro-shrinkage porosity. The triangular micro-shrinkage porosity has a significant impact on mechanical properties.

It is found that the micro-shrinkage porosity is related to the riser neck diameter during ingot preparation by comparing the micro-shrinkage porosity in Figure 4. When $\phi A = 20 \text{ mm}$, the triangular micro-shrinkage porosity is smaller, as shown by the white arrow in Figure 4(b). The micro-shrinkage porosity is mainly polygonal and vermicular,

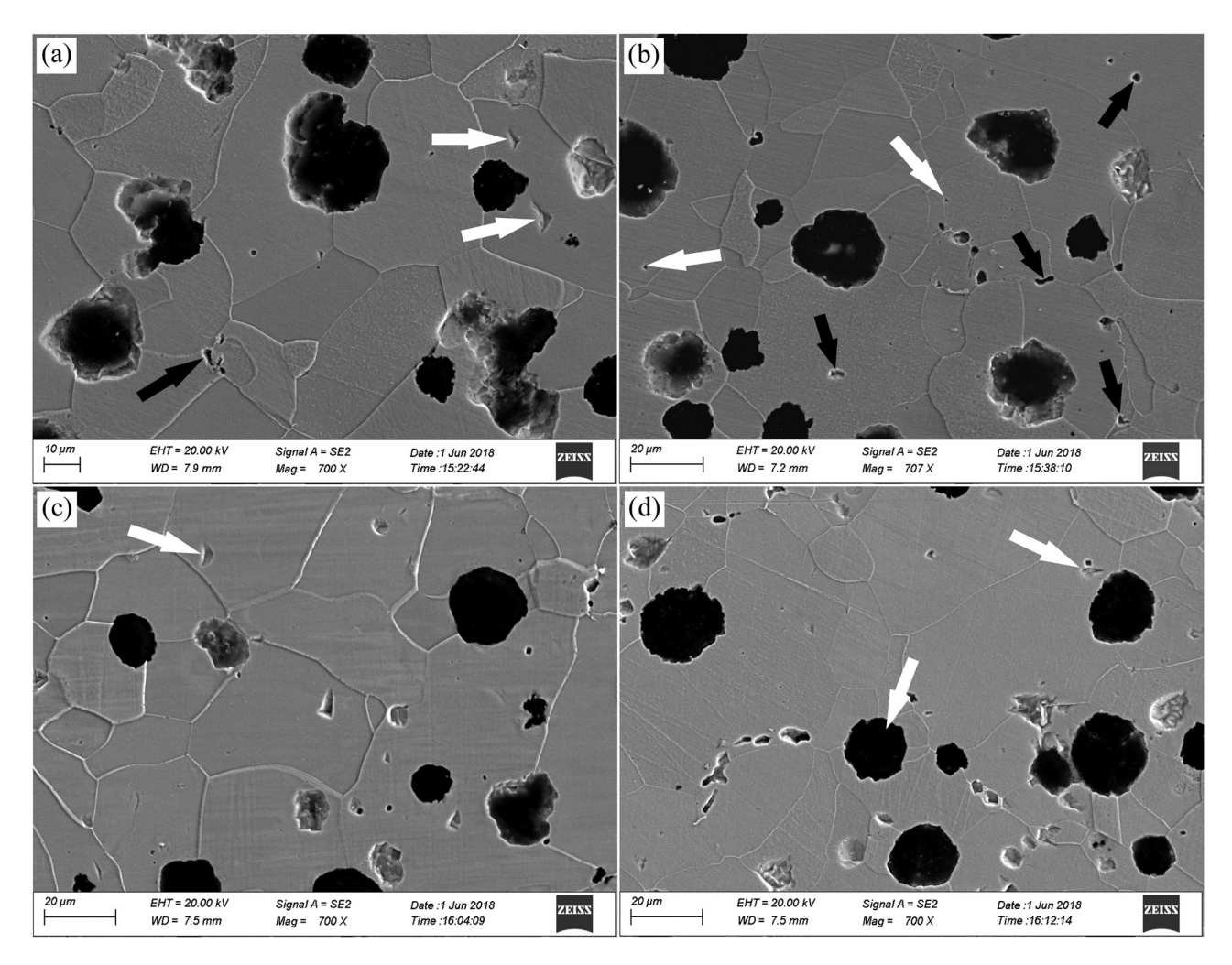


Figure 4: SEM images of $\frac{1}{2}$ radius away from the cast center: (a) $\varphi A = 15$; (b) $\varphi A = 20$; (c) $\varphi A = 25$; (d) $\varphi A = 30$.

as shown by the black arrow in Figure 4(b). For other riser neck diameters, the size and quantity of triangular microshrinkage porosity are larger. Accordingly, when casting ingots with a diameter of 70 mm and a height of 110 mm by metal mold, the formation of triangular micro-shrinkage porosity can be effectively inhibited when $\phi\,A=20$ mm.

Ten fields of view are randomly selected for each sample. The results are shown in Table 2. Depending on the measurement results, the size of the triangular microshrinkage porosity in the ingot is the smallest, which is about $2.7\,\mu m$ when the diameter of the ingot riser neck shown in Figure 1 is 20 mm. It is consistent with the qualitative results observed in Figure 4.

2.2.2 Effect of cooling rate on micro shrinkage porosity

The effect of cooling rate on micro-shrinkage porosity was characterized by the distribution of micro-shrinkage porosity on the ingot radius. SEM images of samples at

different positions on the same radius of ingot when ϕ A is 20 mm are shown in Figures 5 and 4(b). It can be seen that there are many significant micro-shrinkage porosities in the center of the ingot by comparing Figures 5 and 4(b), as shown in Figure 5(a). There is less and smaller micro-shrinkage porosity at the edge of the ingot, as shown in Figure 5(d). The number of triangular micro-shrinkage porosities is increasing, and the size of them is getting bigger with the decrease of the distance to the center of the ingot. The cooling speed at the edge of the ingot is fast and the cooling speed at the center is slow, so the above changes in micro-shrinkage porosity are caused by the cooling speed. Therefore, it can be seen that increasing the cooling speed plays an auxiliary role in reducing the micro-shrinkage porosity in nodular cast iron.

2.3 Low-temperature impact toughness

The test results of the impact energy of samples at -40 to -70°C are shown in Figure 6.

Table 2: Test results of impact energy of triangular micro-shrinkage porosity with different sizes

| Riser diameter (mm) Micro-shrinkage porosity length λ (μ m) | | 15 | 20 | 25 | 30 14.3 ^{+4.1} _{-3.4} | |
|---|-------|---------------------|---------------------|------------------|--|--|
| | | 8.8 ^{+1.9} | $3.7^{+2.6}_{-1.2}$ | 13.6+3.2 | | |
| $a_{\rm k}~({\rm J}~{\rm cm}^{-2})$ | -40°C | 13.55 ± 0.15 | 13.5 ± 0.4 | 13.20 ± 0.0 | 12.80 ± 0.1 | |
| | −50°C | 12.95 ± 0.25 | 13.05 ± 0.05 | 12.2 ± 0.2 | 12.35 ± 0.15 | |
| | -60°C | 11.90 ± 0.1 | 12.85 ± 0.25 | 11.15 ± 1.05 | 11.0 ± 0.1 | |
| | −70°C | 10.05 ± 0.05 | 12.0 ± 0.50 | 8.85 ± 0.05 | 8.35 ± 0.15 | |

2.3.1 Effect of the temperature

It can be seen in Figure 6 that the impact energy decreases slowly at first and then increases quickly with the decrease in temperature. When the temperature decreases from -40 to -50°C, the reduction value of impact energy of each sample is about 0.5 J, indicating that the change of impact energy is minimal within this temperature range. When the temperature decreases from -50 to -60°C, the reduction of the impact energy is more than 1 J, and the sensitivity of impact energy to temperature is strengthened. When the temperature decreases from -60 to -70°C, the

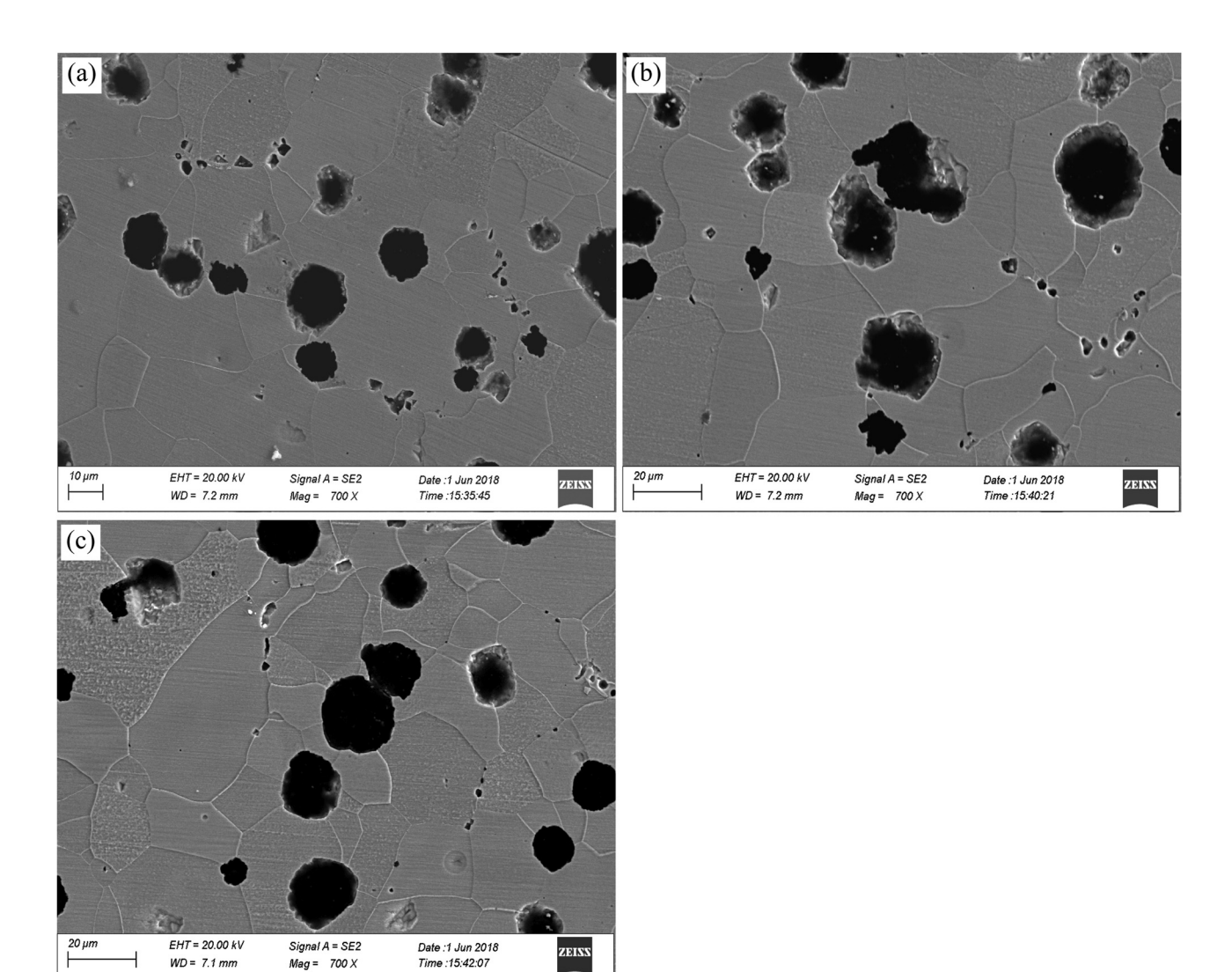


Figure 5: Distribution of the micro-shrinkage porosity of the ingot when φ A is 20 mm: (a) center part; (b) ²/₃ radius away from ingot center; (c) edge.

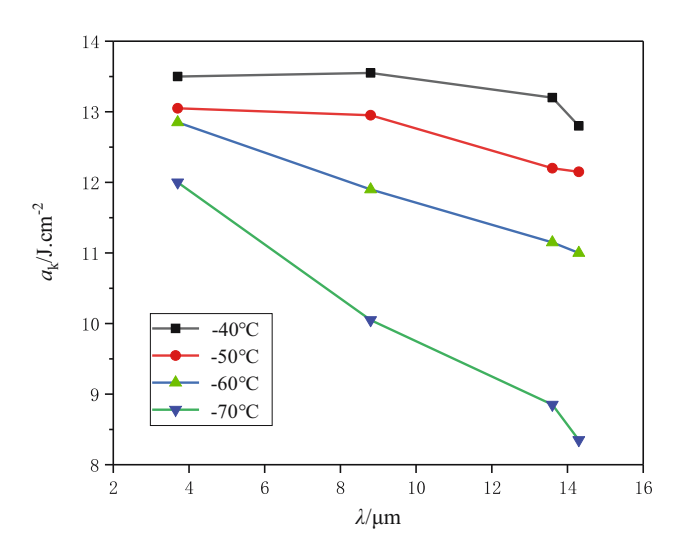


Figure 6: Variation of impact energy with temperature and microshrinkage porosity.

reduction of impact energy of most samples exceeds 2 J, and the effect of temperature on impact energy is more obvious.

2.3.2 Effect of micro-shrinkage porosity

The experimental results in Figure 6 show that the impact energy of ferrite iron generally decreases with the increase in the size of the micro-shrinkage porosity. The lower the temperature, the more obvious the impact energy is affected by the size of micro-shrinkage porosity.

When the average length of micro-shrinkage porosity is 3.7 μ m and the temperature is –70°C, the impact energy can still reach 12 J. When the temperature decreases from –40 to –70°C, the impact energy only decreases by 1.5 J, which is shown in Table 2.

If the temperature below -40°C is defined as ultra-low temperature, it can be determined according to Figure 6 and Table 2 that micro-shrinkage porosity at ultra-low temperature has a significant impact on impact energy. The lower the temperature is, the more serious the impact is.

3 Discussion

3.1 Correlation between micro-shrinkage porosity and riser neck diameter of nodular cast iron

It is an effective method to reduce or eliminate the microshrinkage porosity of nodular cast iron in which the pressure generated by the graphitization expansion of molten iron acts on the austenite surrounding the graphite nodule to promote the deformation of austenite. Forming pressure by using graphitization expansion in molten iron requires two conditions. One is that the mold has sufficient stiffness. The other is that the molten iron is in a closed container during graphitization expansion. In order to satisfy two conditions, metal mold casting must be used, and the liquid shrinkage and riser neck diameter solidification should end at the same time. Therefore, the microshrinkage porosity of nodular cast iron is related to the diameter of the riser neck in metal mold casting.

3.1.1 Appropriate riser neck diameter is helpful in reducing or eliminating micro-shrinkage porosity

The appropriate riser neck diameter means that the liquid shrinkage of the molten iron and the solidification of the riser neck end at the same time, causing the molten iron to precipitate graphite nodules in the closed cavity, and the pressure is formed in the molten iron during graphitization expansion. This pressure forces the austenite surrounding the graphite nodule to deform and fill the gap between austenites. When the pressure is large enough, micro-shrinkage porosity can be completely eliminated, as shown in Figure 7(b). In the experiment, when $\phi\,A=20$ mm, the size of micro-shrinkage porosity decreases obviously and the shape changes obviously, as shown in Figure 4(b), indicating that the riser neck diameter is relatively appropriate.

3.1.2 Inappropriate riser neck diameter has little effect on the micro-shrinkage porosity

If the riser neck diameter is too small, the riser neck will solidify when the liquid does not shrink or is shrinking. Although a closed cavity is formed, the cavity is not filled because the molten iron continues to shrink. If the expansion caused by the precipitation of graphite nodule cannot fill the mold cavity, the pressure cannot be generated in the molten iron. Micro-shrinkage porosity is formed after solidification, as shown in Figure 7(a). If the expansion caused by the precipitation of graphite nodule can fill the cavity, the pressure will be generated in the molten iron. Although the pressure is small at this time, it will help reduce the size of micro-shrinkage porosity. When ϕ A is 15 mm, the micro-shrinkage porosity decreases slightly in the experiment, which is considered to be caused by the relatively small diameter of the riser neck, as shown in Figure 4(a).

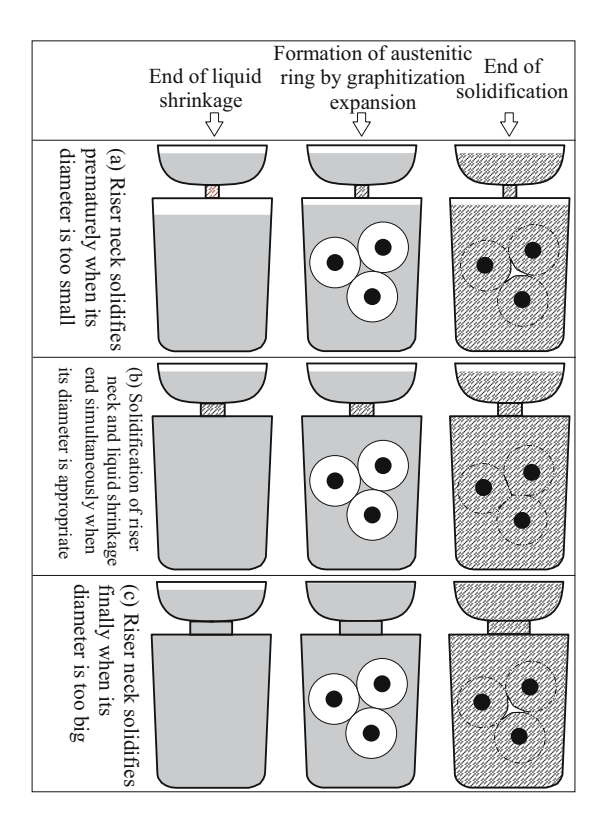


Figure 7: Schematic diagram of the formation process of microshrinkage porosity of nodular cast iron.

If the diameter of the riser neck is too large, the part of the riser neck will finally solidify. The expansion force generated by the precipitation of graphite causes the molten iron in the mold cavity to flow back into the riser. There is no pressure in the molten iron, and microshrinkage porosity is formed after solidification, as shown in Figure 7(c). When the value of ϕ A is larger than 20 mm, the amount and the size of the micro-shrinkage porosity are large owing to the large diameter of the riser neck in the experiment, as shown in Figure 4(c) and (d).

3.2 Micro-shrinkage porosity becomes one of the key factors affecting the impact toughness of nodular cast iron at ultralow temperatures

It is generally believed that the finer and rounder the graphite ball is, the higher the low-temperature impact toughness is for the ferritic ductile iron. However, comparing the experimental results of Figures 2 and 3 and and 6, it is found that the change in impact energy at ultralow temperatures is not caused by the graphite ball. The reason is that when $\phi\,A=15\,\text{mm}$ and $\phi\,A=25\,\text{mm}$, the graphite ball is finer and rounder, but the impact energy is

lower. When ϕ A = 20 mm, although the graphite ball is large, the low-temperature impact energy is the highest. It can be seen from Figure 2 that the number and size of ferrite grains are basically the same, so the change in impact energy at ultra-low temperatures is not caused by the ferrite matrix.

By comprehensively comparing the experimental results in Figures 2–6 and combining them with the above analysis, it can be determined that micro-shrinkage porosity causes the change in impact energy of ferrite matrix nodular cast iron at low temperatures. The lower the temperature is, the more obvious the role of micro-shrinkage porosity is. Micro-shrinkage porosity becomes one of the key factors affecting the impact toughness of nodular cast iron at ultra-low temperatures.

Zhang et al. [22] believe that the formation of cracks controls the low-temperature impact fracture process of ferritic nodular cast iron. The lower the temperature is, the more obvious the role of the crack formation process is. It can be seen in Figure 4 that the radius of curvature of the triangular micro-shrinkage tip is much smaller than that on the convex edge of the graphite nodule. Under the action of an external force, the crack is first formed at the triangular micro-shrinkage porosity. Therefore, when crack formation becomes the key link in the fracture process, the micro-shrinkage porosity will automatically change into the key factor affecting the impact toughness of nodular cast iron.

4 Conclusions

- (1) The number and size of triangular micro-shrinkage porosity can be reduced by changing the riser neck diameter when casting nodular cast iron in a metal mold. The triangular micro-shrinkage porosity can be transformed at the same time into a polygon or worm shape.
- (2) The impact energy of nodular cast iron decreases with an increase in micro-shrinkage porosity size. The greater the effect of the size of micro-shrinkage porosity on impact energy, the lower the temperature. When the spheroidization rate of ferrite-based nodular cast iron is more than 98% and the number of graphite nodules is more than 810 mm⁻², the micro-shrinkage porosity becomes the key factor affecting the ultra-low temperature impact toughness of nodular cast iron. When the length of micro-shrinkage porosity is less than 3.7 μm, the impact energy of ferrite-based nodular cast iron can still reach more than 12 J at −70°C.

Acknowledgments: In writing this paper, I have benefited from the presence of my colleagues. They generously helped me collect materials I needed and made many invaluable suggestions. I hereby extend my grateful thanks to them for their kind help, without which this paper would not have been what it is.

Funding information: The authors acknowledge the financial support provided by major science and technology projects in Liaoning Province, China (Approval No.: 1585015895240)

Author contributions: Shuying Chen, Guowei Chang, Qingchun Li: Conception and design of the study, drafting and revising the article, final approval of the version to be published. Ming Sun, Jiajian Song, Haiqing Sun: Acquisition of data, analysis and interpretation of data, final approval of the version to be published.

Conflict of interest: Authors state no conflict of interest.

References

- [1] Toktas, G., A. Toktas, and M. Tayanc. Influence of matrix structure on the fatigue properties of an alloyed ductile iron. Materials and Design, Vol. 29, No. 8, 2008, pp. 1600-1608.
- [2] Zhang, K., J. D. Liu, X. F. Song, L. Y. Li, S. B. Qi, Z. L. Ning, et al. Investigation on low-temperature impact toughness of heavysection nodular iron. Modern Cast Iron, Vol. 37, No. 3, 2017, pp. 41-45.
- [3] David, P., J. Massone, R. Boeri, and J. Sikora. Mechanical properties of thin wall ductile iron-influence of carbon equivalent and graphite distribution. ISIJ International, Vol. 44, No. 7, 2004, pp. 1180-1187.
- [4] Caldera, M., J. M. Massone, R. E. Boeri, and J. A. Sikora. Impact properties of thin wall ductile iron. ISIJ International, Vol. 44, No. 4, 2004, pp. 731-736.
- Torsten, S. G. and L. S. Ingvar. The effect of graphite fraction and morphology on the plastic deformation behavior of cast irons. Metallurgical and Materials Transactions A, Vol. 38, No. 4, 2007, pp. 840-847.
- Iacoviello, F. and V. D. Cocco. Influence of the graphite elements morphology on the fatigue crack propagation mechanisms in a ferritic ductile cast iron. Engineering Fracture Mechanics, Vol. 167, No. 11, 2016, pp. 248-258.
- [7] Nuno, C., M. Nuno, and S. F. Samuel. Influence of graphite nodules geometrical features on fatigue life of high-strength nodular cast iron. JMEPEG, Vol. 17, No. 3, 2008, pp. 352-362.
- Chen D, W. W. Sang, L. X. Wu, M. H. Yan, and P. K. Wang. Study on thermal fatigue crack initiation and propagation behavior in

- nodular cast iron. Foundry Technology, Vol. 39, No. 2, 2018, pp. 482-432.
- [9] Diao, X. G., Z. L. Ning, F. Y. Cao, S. Z. Ren, and J. F. Sun. Graphite morphology evolution during melt holding of ductile iron. Key Engineering Materials, Vol. 457, 2011, pp. 31-36.
- [10] Shin, W. S., S. Baek, and Y. J. Kim. Effect of Sn addition on the microstructure and friction-wear properties of a nodular graphite cast iron. Korean J Met Mater, Vol. 60, No. 6, 2022, pp. 471-477.
- [11] Lacaze, J., P. Larrañaga, I. Asenjo, R. Suarez, and J. Sertucha. Sertucha Influence of 1 wt% addition of Ni on structural and mechanical properties of ferritic ductile irons. Materials Science and Technology, Vol. 28, No. 5, 2012, pp. 603-608.
- [12] Sun, Y. F., S. M. Hu, Z. Y. Xiao, S. S. You, J. Y. Zhao, and Y. Z. Lv. Effects of nickel on low-temperature impact toughness and corrosion resistance of high-ductile iron. Materials and Design, Vol. 41, 2012, pp. 37-42.
- [13] Zhang X. N., Y. D. Qu, H. W. Yang, and R. D. Li. Temperature impact toughness and fracture mechanism of cast QT400-18L ductile iron with different Ni additions. China Foundry, Vol. 10, No. 5, 2013, pp. 310-314.
- [14] Chen X. R., J. Xu, H. R. Hu, H. Mohrbacher, M. Kang, W. Zhang, et al. Effects of niobium addition on microstructure and tensile behavior of as-cast ductile iron. Materials Science and Engineering A, Vol. 688, No. 3, 2017, pp. 416-428.
- [15] Sckudlarek, W., M. N. Krmasha, K. S. A. Rubaie, O. Preti, J. C. G. Milan, and C. E. Costa. Effect of austempering temperature on microstructure and mechanical properties of ductile cast iron modified by niobium. Journal of Materials Research and Technology, Vol. 12, 2021, pp. 2414-2425.
- [16] Costa, N., N. Machado, and F. S. Silva. A new method for prediction of nodular cast iron fatigue limit. International Journal of Fatique, Vol. 32, 2010, pp. 988-995.
- [17] Borsato, T., P. Ferro, F. Berto, and C. Carollo. Fatigue strength improvement of heavy-section pearlitic ductile iron castings by in-mould inoculation treatment. International Journal of Fatigue, Vol. 102, 2017, pp. 221-227.
- [18] Verdu, C., J. Adrien, and J. Y. Buffière. Three-dimensional shape of the early stages of fatigue cracks nucleated in nodular cast iron. Materials Science and Engineering A, Vol. 483-484, 2008, pp. 402-405.
- [19] Verdu, C., J. Adrien, and A. Reynaud. Contributions of dual phase heat treatments to fatigue properties of SG cast irons. International Journal of Cast Metal Research, Vol. 18, No. 6, 2005, pp. 346-354.
- [20] Guo, E. J. Effect of Ce-Mg-Si and Y-Mg-Si nodulizers on the microstructures and mechanical properties of heavy section ductile iron. Journal of Rare Earths, Vol. 32, No. 8, 2014, pp. 38-744.
- [21] Gao, M. Q., G. L. Li, and J. H. You. Cementites decomposition of a pearlitic ductile cast iron during graphitization annealing heat treatment. Journal of Iron and Steel Research International, Vol. 24, 2017, pp. 838-843.
- [22] Zhang, X., Y. Qu, R. Li, and J. You. Mechanism of crack nucleation and propagation of ferrite ductile iron during impact fracture under low temperatures. Acta Metallurgica Sinica, Vol. 51, No. 11, 2015, pp. 1333-1340.